

**Premixed Carbon Monoxide-Nitrous Oxide-Hydrogen Flames:
Measured and Calculated Burning Velocities with and without Fe(CO)₅¹**

Gregory T. Linteris, Marc D. Rumminger and Valeri I. Babushok
Building and Fire Research Laboratory
National Institute of Standards and Technology, Gaithersburg MD 20899, USA

To appear in *Combustion and Flame*

Full-length article

Running title: CO-N₂O Flame Speeds with Iron Pentacarbonyl

Corresponding author:

Gregory T. Linteris
National Institute of Standards and Technology
Building 224, Room B356, Stop 8651
Gaithersburg MD 20899-8651, USA
linteris@nist.gov
ph: 301-975-2283
fax: 301-975-4052

¹ Official contribution of the National Institute of Standards and Technology, not subject to copyright in the United States.

Premixed Carbon Monoxide-Nitrous Oxide-Hydrogen Flames: Measured and Calculated Burning Velocities with and without Fe(CO)₅

Gregory T. Linteris², Marc D. Rumminger³, and Valeri Babushok

Building and Fire Research Laboratory
National Institute of Standards and Technology
Gaithersburg MD 20899, USA

To appear in *Combustion and Flame*

ABSTRACT

The burning velocity of premixed carbon monoxide-nitrous oxide flames (background water levels of 5 to 15 ppm) has been determined experimentally for a range of fuel-oxidizer equivalence ratio ϕ from 0.6 to 3.0, with added nitrogen up to a mole fraction of $X_{N_2} = 0.25$, and with hydrogen added up to $X_{H_2} = 0.005$. Numerical modeling of the flames based on a recently developed kinetic mechanism predicts the burning velocity reasonably well, and indicates that the direct reaction of CO with N₂O is the most important reaction for CO and N₂O consumption for values of $X_{H_2} \leq 0.0014$. The calculations show that a background H₂ level of 10 ppm increases the burning velocity by only about 1 % compared to the bone-dry case. Addition of iron pentacarbonyl, Fe(CO)₅, a powerful flame inhibitor in hydrocarbon-air flames, *increases* the burning velocity of the CO-N₂O flames significantly. The promotion is believed to be due to the iron-catalyzed gas-phase reaction of N₂O with CO, via $N_2O + M = N_2 + MO$ and $CO + MO = CO_2 + M$, where M is Fe, FeO, or FeOH.

² Corresponding author, linteris@nist.gov

³ National Research Council/NIST postdoctoral fellow, 1996-1999; current address: Sandia National Lab, MS9052, Livermore CA, 94551

INTRODUCTION

The present investigation was conducted for the dual purposes of studying the effectiveness of the flame inhibitor iron pentacarbonyl in non-branching chain flames of CO and N₂O, and to investigate the role of the direct reaction of CO with N₂O at flame temperatures with controlled amounts of hydrogen. The most effective chemical flame inhibitors are believed to act through catalytic cycles that recombine radicals in the flame. These inhibitors, however, have not been tested in systems without chain branching. In addition, we are also responding to the need described by Allen et al. [1] for burning velocity measurements in the CO-N₂O system to assess the role of the direct reaction under dry conditions at flame temperatures.

The high-temperature gas-phase reactions of carbon monoxide and nitrous oxide are an important and well-studied system. These reactions occur in the gas-phase region during combustion of nitramine-based solid rocket propellants [2-4], and they are also important for understanding the combustion emission characteristics of stationary and mobile power plants. The direct reaction of CO with N₂O is of fundamental interest since it is one of the simplest examples of an exchange reaction between saturated molecules. For inhibition studies, the reactant mixture provides a non-chain mechanism involving oxygen atoms, so that the significance of catalytic O-atom recombination cycles of iron species from the inhibitor can be tested, as well as those of H and OH when trace hydrogen is added as a reactant.

The CO-N₂O reaction has been studied in shock tubes [5-7] and flow reactors [1]. Loirat et al. [8] measured the critical ignition pressure of CO-N₂O mixtures in a cylindrical reactor. In flame studies, Dindi et al. [9] measured the stable species mole fractions in low-pressure premixed flames using gas chromatography, and Vandooren et al. [10] recently used mass spectrometry to measure the structure of CO-N₂O-H₂ flames. Cor et al. [11] measured the stable species profiles in low-pressure counterflow CO-N₂O-N₂

diffusion flames. These studies have provided data for determining elementary rates and for testing comprehensive mechanisms. In many of the studies, the possible interference of H-atom reactions from impurities has been described, but not always quantified.

The burning velocity of premixed CO-N₂O flames has been measured previously in three investigations. Van Wouterghem and Van Tiggelen [12] measured the flame speed of lean, stoichiometric, and rich flames, some with nitrogen dilution, having estimated hydrogen impurities of less than 2000 ppm⁴ in the CO (but not noted for the N₂O). Kalff and Alkemade [13] provided data on stoichiometric and rich flames with up to 10 % added water vapor, and a minimum hydrogen content estimated to be less than 500 ppm. Simpson and Linnett [14] investigated quite rich systems ($\phi = 2.0$), diluted by nitrogen, with unquantified, but low, levels of hydrogen impurities. The burning velocity of premixed CO-N₂O flames has been calculated [1,15], but the absence of data for flames with low hydrogen content was noted in both studies.

Since the levels of hydrogen are somewhat high or unquantified in previous experiments, additional experiments are required to understand the importance of the direct reaction at flame temperatures. We report burning velocity measurements for stoichiometric CO-N₂O flames with added H₂ mole fractions from 0 ppm to 6800 ppm. For the driest conditions (5 to 15 ppm H₂O), we also report flame speeds for equivalence ratios from 0.6 to 3.0, and for stoichiometric flames with nitrogen dilution up to 25 % of the total volumetric flow. For all conditions, the flame structure is numerically calculated using a detailed chemical kinetic mechanism, providing an estimate for the rate of the direct reaction at the flame temperature, and allowing assessment of the relative importance of the different reaction routes for consumption of N₂O and CO.

⁴ all references to ppm in this paper are on a volume basis and refer to $\mu\text{l/l}$.

The CO-N₂O flames were also used to study the inhibition mechanism of Fe(CO)₅. There is an urgent need to find replacements for the effective and widely used fire suppressant CF₃Br and related compounds [16]; however, a replacement with all of the desirable properties of CF₃Br is proving difficult to find and research has intensified [17]. Certain metallic compounds have been found to be substantially more effective flame inhibitors than halogen-containing compounds [18-20]. Iron pentacarbonyl is among the most effective flame inhibitors ever identified [18], up to two orders of magnitude more effective than CF₃Br, and recent progress has been made in understanding its mechanism [21]. Although Fe(CO)₅ is flammable and highly toxic and could never be used as a fire suppressant itself, other iron-containing compounds have been identified which are far less toxic and flammable, and which also demonstrate strong flame inhibition [22]. If means can be identified to safely introduce metal species into a fire, they may be beneficial components in a fire suppressant blend, particularly for unoccupied spaces. Further, the fundamental understanding gained from study of these near-ideal inhibitors, which catalytically recombine radicals, provides a theoretical basis for development of new inhibitors.

A detailed chemical kinetic mechanism for iron-species inhibition of flames has been introduced [23], and modeling with the mechanism supports the premise that the inhibition is primarily a gas-phase phenomenon. Numerical calculations using the mechanism predict many of the properties of the flames examined; nonetheless, some of the features of the flames are not well-described, and much work remains to be done to test and validate the mechanism. In particular, inhibition in lean flames (where O-atom reactions are much more important) is not accurately modeled by the mechanism.

In previous research, oxides of nitrogen have been used as the oxidizer in studies of the effectiveness of flame inhibitors [24]. Since systems using nitrogen oxides instead of O₂ undergo non-chain-branching radical reaction sequences, the relative

effectiveness of agents believed to act through catalytic radical recombination cycles may be very different, affording new opportunities to understand the inhibition by $\text{Fe}(\text{CO})_5$.

In the absence of hydrogen, the oxidation mechanism of $\text{CO-N}_2\text{O}$ flames is believed to proceed through either the direct reaction or through the thermal decomposition of N_2O followed by O-atom reaction with N_2O or CO . Recent research with $\text{Fe}(\text{CO})_5$ inhibition of $\text{CO-O}_2\text{-N}_2\text{-H}_2$ flames has shown that in some systems a new O-atom radical recombination cycle may dominate radical destruction [25]. Also, Kaufman [26] has shown that $\text{Fe}(\text{CO})_5$ addition to a flow tube causes very strong reduction in O-atom concentration. The extent to which $\text{Fe}(\text{CO})_5$ affects dry $\text{CO-N}_2\text{O}$ flames will depend upon the predominance of the O-atom route for N_2O and CO consumption and the effectiveness of the iron-catalyzed O-atom radical recombination cycle. Since gas-phase iron is also believed to catalyze the decomposition of N_2O (as discussed below), the relative efficiency of this reaction will also affect the influence of iron in this flame. In summary, in the flame inhibition experiments and modeling, we seek to determine the effectiveness of $\text{Fe}(\text{CO})_5$ in a system which is non-chain branching, to test the postulate that for these systems, radical recombination—even by a very powerful catalytic agent—is not as effective. The results may have implications for the practical problem of the suppression of propellant fires.

EXPERIMENTAL

A Mache-Hebra nozzle burner (inner diameter $1.02 \text{ cm} \pm 0.005 \text{ cm}$) [27] with a schlieren imaging system [28] provides the average burning velocity of these Bunsen-type flames using the total area method [29]. The experimental system has been described in detail previously [30]. Calibrated mass flow controllers meter the gas flows, and a two-stage

saturator adds $\text{Fe}(\text{CO})_5$ as a vapor. The burner produces straight-sided schlieren images that are captured by a video frame-grabber board in a computer. The fuel gas is carbon monoxide (Matheson⁵ UHP, 99.9 % CO, for which a batch analysis by the manufacturer shows the concentration of H_2O and CH_4 to be less than 0.3 ppm and 1.0 ppm, respectively, and an in-house FTIR analysis showed H_2O and HCs to be present at less than 1 ppm each). For some tests, the fuel stream contains added hydrogen (Matheson UHP, 99.999 % H_2 , with sum of N_2 , O_2 , CO_2 , CO, Ar, CH_4 , and H_2O < 10 ppm). The oxidizer stream consists of nitrous oxide (Matheson UHP, 99.99 % N_2O , with sum of N_2 , O_2 , CO, CO_2 , and CH_4 less than 100 ppm, which an in-house FTIR analysis showed to have 25 ppm of H_2O , and less than 4 ppm of the sum of hydrocarbons up to C_4). Added nitrogen is boil-off from liquid N_2 .

The burning velocity in Bunsen-type flames is known to vary at the tip and base of the flame and is influenced by curvature and stretch; however, these effects are most important over a small portion of the flame. In order to minimize the influence of curvature and stretch on interpretation of the action of the chemical inhibitor, we present the burning velocity of *inhibited* flames as a normalized parameter: the burning velocity of the inhibited flame divided by the burning velocity of the uninhibited flame at the same flow conditions.

Uncertainty Analysis

The uncertainty analysis consists of calculation of individual uncertainty components and root mean square summation of components [31], and has been described in detail in a previous publication [32]. All uncertainties are reported as expanded uncertainties: $X \pm U$, (level of confidence approximately 95 %) or relative uncertainties: $U / X \cdot 100 \%$. The

⁵ Certain commercial equipment, instruments, or materials are identified in this paper to adequately specify the procedure. Such identification does not imply recommendation or endorsement by the National Institute

primary sources of uncertainty in the average burning velocity measurement are the 1) accuracy of the flow controllers, 2) determination of the flame area, 3) effect of flame base location on flame area, and 4) location of the schlieren image relative to the cold gas boundary. In general, uncertainty increases with burning velocity. A major source of uncertainty arises from selection of the flame location. Traditionally, the burning velocity of the flame is the flow velocity of the unburned reactants; however, since the schlieren image corresponds to a surface with a temperature above that of the unburned gas [29], use of the schlieren image as the flame area can lead to an underestimation of the burning velocity [33], as compared to the area at the cold-gas boundary. Previous researchers [29,33,34] have attempted to adjust the flame area to the 298 K isotherm (T_{298}), although this generally requires knowledge of the 2-D temperature field in the flame. We do not make such corrections in this paper, and note that it has not yet been done using experimental (rather than calculated) temperature profiles in a flame. Further, some researchers argue for the use of the visible flame area rather than the schlieren area (which would tend to reduce the burning velocities in the present work) [35]. We retain the traditional approach of using the schlieren area, but note that differences on the order of 10% can result from the choice of image to use in the analyses.

Inaccuracies in the flow controllers result in uncertainties of 1.4 % for the equivalence ratio, 1.1 % for the nitrogen mole fraction, and 1.2 % for the hydrogen mole fraction. For stoichiometric mixtures of N_2O and CO , trace hydrogen (as H_2O) is present in the reactant gases at about 13 ppm. Neglecting the uncertainty (unspecified) in the vapor pressure correlation of Gilbert and Sulzmann [36], the uncertainties in the bath temperature, ambient pressure and carrier gas flow rate yield an $Fe(CO)_5$ mole fraction

of Standards and Technology, nor does it imply that the materials or equipment are necessarily the best available for the intended use.

uncertainty of 6.5 %.

NUMERICAL

One-dimensional freely-propagating premixed flames are simulated using the Sandia flame code Premix [37], the Chemkin subroutines [38], and the transport property subroutines [39]. For all of the calculations the absolute tolerance is 10^{-14} , the relative tolerance is 10^{-9} , GRAD is 0.15, and CURV is 0.35. The computational domain is 0 to 50 cm (except when noted). The initial temperature is 298 K and the pressure is one atmosphere. The moist CO-N₂O flames are modeled using the mechanism and thermodynamic data set of Allen et al. [1], from which the species NCN, NCO, CNO, CH, CH₂, CH₃, C₂H, HCCO, HNCO, HOCN, HCNO, H₂CN have been removed (they have been found to be unimportant for the present flames). The resulting reduced mechanism has 20 species and 92 reactions. For all calculations (except where noted) we use the rate for CO+OH \leftrightarrow CO₂+H from Yu et al. [40], and for CO+N₂O \rightarrow CO₂+N₂ from Milks and Matula [6] since they provide reasonable agreement with our data. The chemical mechanism for Fe(CO)₅ inhibition of flames (12 species and 55 reactions) and necessary thermodynamic data are compiled from a variety of sources as described in Rumminger et al. [23].

RESULTS AND DISCUSSION

General Features

Prior to discussing the inhibited flames, we first present findings for the uninhibited flames. Calculations show that the pure CO-N₂O flame has a very large domain due to the slow reaction of CO and NO downstream of the main heat release region. A plot of the major species profiles and temperature of a stoichiometric CO-N₂O flame is shown in

Figure 1. There are three distinct regions in the calculated results. In the first, which extends a few millimeters from the start of the temperature rise, there is very fast reaction of CO with N₂O, and thermal decomposition of N₂O followed by reaction of N₂O with O atoms. In the second region, [NO] is constant, but CO is consumed through its slow reaction with O and O₂. In the third region, NO is consumed. Although no practical flame can support such weak reaction over a domain of two meters, it is of interest to determine how the features of the calculated results over the entire domain influence the comparisons with experimental results from a Bunsen-type flame, which remains quasi-one-dimensional only for a few millimeters.

Table 1 presents some calculated burning velocities $v_{o,num}$, temperatures and peak radical mole fractions for dry, undiluted CO-N₂O flames over a range of ϕ and for stoichiometric flames, over a range of added N₂ and H₂. The adiabatic flame temperature (A.F.T.) is given, as well as the temperature at the location of 99.5 % consumption of N₂O, which roughly corresponds to the end of the region of rapid heat release. The temperature at the location of the peak rate of the CO+N₂O reaction is also listed. For pure CO-N₂O flames with $\phi = 1.0$ and hydrogen addition up to 6800 ppm, or dry flames with $0.6 \leq \phi \leq 1.3$ (the first six lines of Table 1), the A.F.T. is 2830 K \pm 40 K, while for the richest flames ($\phi = 3.2$) and stoichiometric flames with nitrogen dilution, the A.F.T. is significantly lower, 2378 K and 2559 K respectively. As Table 1 shows, however, the calculated peak temperature at the point of 99.5 % N₂O consumption is 240 K to 550 K lower than the adiabatic flame temperature. For flames rich in CO or with added N₂, the adiabatic flame temperature is much lower because of dilution, but the temperature at the point of N₂O consumption is only slightly lower. For flames with added hydrogen, the temperature in the main reaction zone is closer to the final temperature far downstream, since the faster overall reaction rate allows more of the CO

to be consumed before the N_2O is gone. Similarly, at the peak of the $\text{CO}+\text{N}_2\text{O}$ reaction, the temperature is about 1800 K; for flames with 6800 ppm of hydrogen it is about 100 K higher, for rich or lean flames it is about 100 K lower, and with 25 % dilution nitrogen is about 40 K lower. Hence, the temperature at the peak of the $\text{CO}+\text{N}_2\text{O}$ reaction is less sensitive to changes in ϕ , X_{N_2} or X_{H_2} than is the adiabatic flame temperature (which is not nearly achieved in the experimental flames). In the present experiment which has a flame thickness of about 1 mm, the calculated temperatures in the main reaction zone, where most of the fuel and oxidizer consumption occur, are more relevant than the adiabatic flame temperatures (which would only be reached nearly 3 m downstream).

The significant but gradual temperature rise far downstream of the main reaction zone is caused by the slow reaction of the remaining CO with O or O_2 , and from NO consumption. Nonetheless, this additional temperature rise does not have much consequence for the main reaction zone; the thickness is too great to provide a high rate of heat feedback, and the flow field in the experiment does not support such a large, one-dimensional downstream region. Numerical experiments for $0.6 \leq \phi \leq 3.2$ show that turning off the $\text{CO}+\text{O}$ and $\text{CO}+\text{O}_2$ reactions, and the even slower NO consumption reactions, provide a burning velocity within 2 % of those using the entire domain with all reactions included. Calculations were also performed over the entire range of ϕ and X_{H_2} ; for each condition, domains of 2 mm, 3 mm, or 3000 mm all yield calculated burning velocities within 1% of each other, providing further evidence that the slow reactions in the very large domain do not affect the measured or calculated burning velocities of smaller, practical flames.

Unlike CO or CH_4 flames, these $\text{CO}-\text{N}_2\text{O}$ flames do not demonstrate the characteristic radical super-equilibrium. The O, H, and OH mole fractions, X_{O} , X_{H} , and X_{OH} , rise monotonically throughout the computational domain up to the point where the

N₂O is 99.5 % gone. The peak in-flame X_O is about the same as in stoichiometric CH₄-air flames, and about a factor of four lower than in CO-air flames with 1 % H₂. Even with about 0.7 % of added H₂, the peak in-flame X_H in the CO-N₂O flames is still more than two orders of magnitude lower than that for the CH₄ or CO flames, clearly demonstrating the straight-chain character of these flames, and suggesting their utility for testing the effectiveness of chemical inhibitors in non-branching systems.

Burning Velocity of Uninhibited Flames

Figure 2 presents the burning velocity of the premixed CO-N₂O flames from the experiments (symbols) as a function of the hydrogen concentration in the reactants. The 'dry' burning velocity is measured to be 23.1 cm/s \pm 0.6 cm/s and this value increases to about twice that value with 0.5 % of hydrogen. The marginal effect of added H₂ is smaller at higher values of the hydrogen mole fraction. (For the reader's convenience, Table 2 contains the experimental data and uncertainties).

The figure also shows the calculated burning velocity (lines) for various values of the specific reaction rate constant for the reaction $\text{CO} + \text{N}_2\text{O} \rightarrow \text{CO}_2 + \text{N}_2$. The bottom curve does not include the direct reaction in the mechanism, and indicates a burning velocity of 2.9 cm/s with no added hydrogen, clearly illustrating that this reaction is required to reproduce our data. The remaining curves in the figure show the calculated result using the rate expressions of Dindi et al. [9], Milks and Matula [6], Loirat et al. [41], Fujii et al. [7], and Loirat et al. [8]. The value recommended by Dindi et al. overpredicts the burning velocity, with too weak of a dependence on X_{H₂}, while the other expressions underpredict it for all values of X_{H₂}. The expression of Milks and Matula [6] provides a burning velocity which is very close to the present data for low values of X_{H₂}, but which deviates for X_{H₂} \geq 0.2 %. Also shown in the figure are the data of Van Wouterghem and

Van Tiggelen [12] (< 2000 ppm of H₂), and the data of Kalff and Alkemade [13] (<500 ppm H₂O). The present data are in good agreement with the low-hydrogen data of both previous investigations, and provide the additional advantage of a very low background level of hydrogen with a controlled level of added hydrogen. Note that although the data of Kalff and Alkemade are presented on the same figure, the experiments contained H₂O rather than H₂. Based on calculations with either added H₂ or H₂O we estimate that H₂ addition, as compared to H₂O addition, lowers the burning velocity about 10 % at 250 ppm and raises it about 10 % at 7200 ppm. Thus we find that the data of Kalff and Alkemade are in excellent agreement with the present data at low hydrogen content, and approximately within the uncertainty of both experiments if our data are extrapolated to their conditions at 7200 ppm H₂O.

Since the CO+OH reaction becomes increasingly important as the hydrogen content increases, the rate of the CO+OH reaction has a large influence on the ability of the model to predict the experimental data at higher X_{H₂}. Figure 3 presents the calculated burning velocity of the CO-N₂O flames with the direct reaction rate of Milks and Matula [6], but using the CO + OH rate expression of Baulch et al. 1973 [42], Yu et al. [40], Baulch et al. 1992 [43], and Wooldridge et al. [44]. The recommendation of Baulch et al. 1992 [43] significantly over-predicts the burning velocity for our data, while that of Baulch et al. 1973 is slightly lower. The rates of Yu et al. and Wooldridge et al. provide results which are nearly identical for the present conditions, and which are very close to the measured burning velocities. Although this rate is important for predicting the dependence of the burning velocity on the added hydrogen, it is not important for predicting the burning velocity of the driest flames here (less than 15 ppm H₂O). For the remainder of the calculations in the present paper, we retain the rate of Yu et al. for CO + OH.

The suggested rate expressions for the direct reaction include those with a high activation energy (e.g. [5,8,41]) and those with a low value (e.g. [6,7,45]). An Arrhenius plot for some of the literature values of the direct reaction is shown in Figure 4. Since the flame temperature in the main reaction zone of the flames varies by about 260 K, the different activation energies can affect the shape of the burning velocity curves in Figure 2 (comparing for example the curves for Loirat et al. 1987 and Fujii, which are fairly close at $X_{H_2}=0$). In order to obtain some temperature variation while avoiding the complications from uncertainty in the CO+OH rate, we examine dry (5 - 15 ppm H_2) flames with inert additive or over a range of ϕ .

Figure 5 presents the burning velocity of the dry flames with added nitrogen up to about 25 % together with calculations using the rate expressions of Loirat et al. [41] and Milks and Matula [6]. Also shown in the figure are the predictions when the pre-exponential factors of the direct reaction rates have been adjusted to provide agreement at $X_{N_2}=0$ (dotted lines). The higher activation energy expression appears to yield too low of a burning velocity with added nitrogen, whereas the lower activation energy expression provides a closer temperature dependence. Van Wouterghem and Van Tiggelen [12] also presented data on the flame speed as a function of X_{N_2} . Although the background hydrogen levels in their experiment are somewhat high (and not measured), their data can still be used to test the present mechanism. (Even with 1000 ppm of H_2 , half the CO consumption occurs via the direct reaction, and the burning velocity is very sensitive to the rate of the direct reaction.) We estimate the background level of H_2 in their reactant mixtures to be that value of X_{H_2} (1560 ppm) which provides a calculated burning velocity which matches their experimental burning velocity for $\phi = 1.0$ and $X_{N_2}=0$. (In the calculation, we use the CO+N₂O rate of Milks and Matula with a 10 % lower pre-exponential, which gives the best fit to our data.) We also show the calculated result

using the rate of Loirat et al., again matched for agreement at $X_{N_2} = 0$. The triangles and the dashed lines in Figure 5 show the data of Van Wonterghem and Van Tiggelen and our calculations. The lower activation energy again provides a closer agreement.

The dependence of the burning velocity on the fuel-oxidizer equivalence ratio ϕ is shown in Figure 6. The experimental results (symbols) for dry flames are presented along with the calculated results (solid lines), again using the direct reaction rate expressions of Loirat et al. [41] and Milks and Matula [6]. As shown previously in Figure 2, the expression of Loirat et al. [41] (along with most of the others) provides a burning velocity significantly lower than the present data for dry flames. When the pre-exponential factor in the direct exchange reaction rate is adjusted to give agreement at $\phi = 1.0$ (dotted lines in the figures), the high activation energy rate of Loirat et al. under-predicts the burning velocity for richer flames (which have lower temperature) more than does the low-activation energy rate of Milks and Matula (note from Table 1 that at $\phi = 3.2$, the peak flame temperature within the primary reaction zone drops by about 200 K compared to its peak at $\phi = 1.0$). Nonetheless, the rate expression of Milks and Matula over-predicts the burning velocity by about 18 % at $\phi = 0.6$, and under-predicts it by about 25 % at $\phi = 3.0$. The data of Van Wonterghem and Van Tiggelen [12] for flames with $X_{H_2} \leq 2000$ ppm are also shown in Figure 6. The dashed line shows the calculated burning velocity for 1560 ppm (as described above). As with our data, the calculations slightly overpredict the flame speed for lean flames and underpredict it for rich flames.

For the given mechanism, over the range of ϕ in Figure 6, the burning velocity is only significantly sensitive to the rate of the exchange reaction (as described below). We have attempted to modify the rate of the next most sensitive reactions (including the rates of the reactions: $N_2O + M$, $N_2O + O$, and $CO + O$) to improve agreement over ϕ ; however, adjustment of these rates within their uncertainty does not improve agreement

in Figure 6. Also, addition of H_2 impurity at 100 ppm, while raising the burning velocity 10 % to 15 % at all values of ϕ , does not affect the qualitative variation with ϕ .

Finally, Figure 7 presents the experimental burning velocity data of Simpson and Linnett [14] for rich ($\phi = 2.0$), slightly pre-heated ($T_{in}=323$ K) CO-N₂O flames with 25 % dilution nitrogen and added water vapor up to about 5 % (error bars estimated here based on ref. [29]). The calculated results for the same initial conditions are shown by the solid line. The agreement is reasonable considering possible differences in the straight tube/flame angle method of determining the burning velocity relative to the nozzle burner/total area method used here.

The numerical modeling of our experimental flame requires the use of the direct reaction for prediction of burning velocity, and the flame results of earlier researchers are also reasonably modeled using the rates suggested in the present work. The kinetic mechanism of Allen et al. [1] provides reasonable agreement with the flame data, while use of the CO + OH rate of Yu et al. [40] or Wooldridge et al. [44] and the CO + N₂O rate of Milks and Matula [6] provide improved agreement. Lowering the pre-exponential factor of the CO + N₂O reaction rate constant of Milks and Matula by about 10% provides the best agreement with our data for dry conditions. Using this rate, the temperature dependence is reasonably modeled, the burning velocity of lean flames ($\phi=0.5$) is overpredicted by about 18%, and that of rich flames ($\phi=3.0$) is underpredicted by about 25 %. The flame results imply a rate of $10^{9.2} \text{ cm}^3 / \text{mol s}$ at 1800 K for the direct reaction, with an activation energy near 71 kJ/mol. Since the direct reaction dominates the reaction system even more so under rich conditions (as described below), it is perhaps more reasonable to infer the direct reaction rate from the burning velocity at $\phi=3.0$. Do this implies a reaction rate of $10^{9.3} \text{ cm}^3 / \text{mol s}$ at 1800 K, or about 30 % higher than the Milks and Matula rate.

The important reactions in the CO-N₂O flames with and without added hydrogen can now be examined using the kinetic mechanism described above. These calculations use the recommendation of Milks and Matula [6] for the direct reaction of CO with N₂O. In Figure 8, the fractional flux of CO (dotted lines) is shown for each important reaction as a function of the mole percent hydrogen. The fractional consumption flux is the fraction of the total consumption of a species occurring due to a given reaction. The total flux for a species is determined by integrating each consumption reaction over the domain of interest (the cold boundary to the point of 99.5 % N₂O consumption), and summing the contribution from each reaction. The fractional flux is the flux for a specific reaction divided by the total flux. As indicated, the direct exchange reaction accounts for about 96 % of CO consumption for the dry condition, decreasing rapidly to about 50 % at 1000 ppm, with a more gradual decrease for greater hydrogen concentrations. Correspondingly, the fraction of CO consumption due to reaction with OH increases. For the reasonably small domain of these calculations (about 2 mm), reactions of CO with O or O₂ (not shown) are at most a few percent of the total consumption flux for CO. The reaction of N₂O is more varied, and the fractional consumption flux of N₂O is shown by the solid lines in Figure 8. Thermal decomposition accounts for about 30 %, and is weakly dependent on the hydrogen concentration. Likewise, reactions of N₂O with O atom to form 2NO or O₂ and N₂ account for about 13 % each, while reactions with NO (not shown) account for a few percent; all of these reactions vary little with X_{H₂}. The contribution of the reaction of N₂O with hydrogen radical (produced from the CO+OH->CO₂+H reaction) increases rapidly as X_{H₂} approaches 1000 ppm and more slowly above that value, with the reaction of N₂O with CO again decreasing correspondingly. A main feature of these flames is that while

hydrogen has a large effect on the reaction mechanism, the direct reaction still accounts for half of the CO consumption and a quarter of the N₂O consumption at X_{H₂} = 1000 ppm.

In Figure 9 , a similar plot is shown for CO and N₂O consumption as a function of ϕ . In these dry flames (5 to 15 ppm H₂O) the direct reaction of CO and N₂O is always responsible for about 96 % of the CO consumption; however, for N₂O consumption, its contribution varies from about 33 % for lean flames to 80 % for the rich flames. Similarly, the contributions of other reactions for N₂O consumption decrease when CO is present in abundance.

Effect of Fe(CO)₅ on CO - N₂O Flames

In order to study the action of chemical inhibitors in systems without radical chain branching, previous researchers have employed nitrogen oxides as the oxidizers. In studies of H₂-N₂-N₂O flames inhibited by CF₃Br and HBr, Dixon-Lewis et al. [46] found the nitrous oxide flames to be inhibited much more weakly than hydrogen-air flames. Similarly, Rosser et al. [24] found that neither CH₄ - NO₂ nor C₂H₄ - NO₂ flames were significantly inhibited by HBr. They further postulated that any flames in which NO₂ is present in significant quantities will not be inhibited by HBr. In studies of moist CO - O₂ and CO - N₂O flames with chlorine, Palmer and Seery [47] predicted that after initial inhibition, further addition of Cl₂ would accelerate the N₂O decomposition, and that CO would then react with ClO; however, they provided no burning velocity data for such flames, and stated that the flames are still ultimately inhibited by chlorine. To further understand the effect of Fe(CO)₅ on radical recombination, particularly in non-branching systems, it is of interest to study its effect in dry and moist CO - N₂O flames. Since Fe(CO)₅ is about 200 times more effective as a flame inhibitor than is Cl, it is of interest to determine if the region of inhibition that Palmer and Seery suggested would occur for

low Cl_2 mole fraction, as well as the ultimate inhibition that they described, may be modified for $\text{Fe}(\text{CO})_5$.

Figure 10 shows the experimental data (symbols) for the burning velocity of N_2O flames with added $\text{Fe}(\text{CO})_5$, normalized by the burning velocity with no inhibitor. Data are provided for added H_2 mole fractions X_{H_2} of 0, 0.001 and 0.002 (note that the background water is 15 ppm). Unlike flames of CH_4 -air, and CO -air which are inhibited by $\text{Fe}(\text{CO})_5$, the overall reaction rates of these CO - N_2O flames are increased. As the figure shows, for hydrogen-free flames with 171 ppm of $\text{Fe}(\text{CO})_5$, the burning velocity is increased by 25 %; as the amount of hydrogen is increased, the rate of burning velocity increase is smaller. In order to understand the reasons for the promotion of the reactions, and also the reduction in this promotion, the flames were modeled as described below.

A mechanism for $\text{Fe}(\text{CO})_5$ -inhibition of hydrocarbon and carbon monoxide flames [23,25] indicates that for those systems, the inhibition occurs due to gas-phase catalytic cycles in which H- or O-atoms are recombined by iron oxide and hydroxide species. Using this mechanism, calculations for the present flames do not show promotion. Recent research in atmospheric chemistry, however, suggests that interactions between Fe-species, N_2O , and CO may be important. West and Broida [48] observed that nitrous oxide destruction is catalyzed by Fe, producing chemiluminescent FeO . Rates for the reaction $\text{Fe} + \text{N}_2\text{O} \rightarrow \text{FeO} + \text{N}_2$ have been measured by Campbell and Metzger [49] and Plane and Rollason [50]. This reaction alone does not provide promotion; however, with subsequent reaction of FeO and CO , it does. Kappes and Staley [51] proposed a catalytic oxidation cycle involving ions: $\text{Fe}^+ + \text{N}_2\text{O} \rightarrow \text{FeO}^+ + \text{N}_2$ and $\text{FeO}^+ + \text{CO} \rightarrow \text{Fe}^+ + \text{CO}_2$, but reaction of neutral FeO with CO is also possible, and would provide a gas-phase catalytic cycle, with the net reaction: $\text{CO} + \text{N}_2\text{O} \rightarrow \text{CO}_2 + \text{N}_2$

Previous experimental work suggests such catalytic effects. In a shock tube study, Matsuda [52] reports that addition of $\text{Fe}(\text{CO})_5$ to $\text{CO-O}_2\text{-Ar}$ mixtures promotes the oxidation of CO. Also, in a fluidized-bed study of the interactions of compounds of iron with those of nitrogen, Hayhurst and Lawrence [53] argue that iron acts as a catalyst to convert N_2O to N_2 and CO to CO_2 (but this appears to be a heterogeneous effect). In addition to the cycle above with FeO, estimates of the heats of reaction indicate that cycles with FeO_2 and FeOOH are possible. The rates for the reactions in the iron-catalyzed $\text{CO-N}_2\text{O}$ system are listed in Table 3. The rate of the first reaction in the table is from Plane and Rollason [50], while the others are our estimates. These reactions are added to the iron-species inhibition mechanism described in Ref. [23]. The thermodynamic data for FeOOH (and the related rate expressions) have been updated based on the recent calculations in Ref. [54]. Calculations of the flame structure using this mechanism have been performed for the $\text{N}_2\text{O-H}_2\text{-Fe}(\text{CO})_5$ flames and are described below.

Figure 10 also shows the calculated burning velocity (normalized by the calculated burning velocity in the absence of iron pentacarbonyl) as a function of the initial $\text{Fe}(\text{CO})_5$ mole fraction $X_{\text{Fe}(\text{CO})_5}$ for added hydrogen mole fractions of 0, 0.1 % and 0.2 %. The calculated results show the correct qualitative behavior for $\text{Fe}(\text{CO})_5$ addition to the dry N_2O flames. For the two cases with added hydrogen, a slight difference in the promotion effect is predicted for $X_{\text{H}_2} = 0.001$ or 0.002, but the variation is greater in the experiments. The calculated burning velocity in the moist flames with $\text{Fe}(\text{CO})_5$ is very sensitive to the rates of the catalytic steps involving FeOOH . While changes in these rates do affect the separation of the curves for $X_{\text{H}_2} = 0.001$ and 0.002, they cannot provide agreement between experiment and calculation, and further research is required.

Careful investigation of Figure 10 reveals that for all values of X_{H_2} , the slope of the experimental curve decreases as $X_{Fe(CO)_5}$ increases, but that the calculated curve is linear. The curvature is mild, and ordinarily might not be of interest given the other discrepancies between the measured and predicted flame speeds with added $Fe(CO)_5$. This reduction in the marginal influence of the $Fe(CO)_5$ (reaction *promotion*) as $X_{Fe(CO)_5}$ increases, however, is much like the loss of effectiveness of $Fe(CO)_5$ observed in flames of CH_4 or CO with air, in which the marginal *inhibition* is reduced at higher $Fe(CO)_5$ mole fractions. In previous work, the loss of inhibition effectiveness was argued to be due to the formation of condensed-phase particulates, which serve as a sink for the active gas-phase iron-containing inhibiting species [21]. Through the use of classical laser scattering and extinction measurements with phase-sensitive detection, it was later shown that a large increase in the particle scattering signal was well correlated with the point where the inhibitor lost its marginal effect [55,56]. It is possible that the reduction in the promotion effect in the present flames is also due to loss of the active iron intermediates through condensation. In order to test this hypothesis, we performed laser scattering measurements on premixed $CO-N_2O$ flames with 0 % and 0.2 % added hydrogen and for 0 and 180 ppm of added $Fe(CO)_5$ using the apparatus described in detail in references [55,56]. The experiments show that with addition of iron pentacarbonyl, there was no significant particle scattering signal in the main reaction region for either level of H_2 in the reactants, unlike the hydrocarbon flames in which a significant scattering signal was detected that clearly increased as the mole fraction of $Fe(CO)_5$ increased. Hence, we cannot conclude that the reduction in the promotion effect near $X_{Fe(CO)_5} = 60$ ppm for $X_{H_2} = 0.002$ is due to formation of particulates in the flame.

Although agreement between the measured and calculated normalized burning

velocity in Figure 10 is not perfect, it is still of interest to investigate the numerical results to determine the reasons for the promotion of the reaction (and the lower promotion when hydrogen is present). Reaction flux and sensitivity analyses are used to provide insight. For each important species in the mechanism, Table 4 shows the fractional flux through the reactions contributing more than 1 % to their consumption or production; Table 5 shows the first-order sensitivity coefficient of the burning velocity with respect to the reaction rate constant ($d(\ln v)/d(\ln k) / d(\ln v)/d(\ln k)|_{\max}$). In both of these tables, calculated results are provided for $X_{H_2} = 0$ and 0.002, and for added $Fe(CO)_5$ of 0 ppm and 213 ppm.

Dry Flames

The properties of the dry flames without $Fe(CO)_5$ are as described above. As Table 4 shows, ninety-four percent of the CO is consumed by the direct reaction, while N_2O consumption is roughly equally portioned between thermal decomposition, the direct reaction, and reaction with O atoms. In Table 5, the burning velocity of the iron-free dry flames is most sensitive to the rate of the direct reaction, followed by the decomposition of N_2O , and to a lesser extent its reaction with O. Upon addition of iron species, 32 % of the CO is consumed through reaction with FeO or FeO_2 , which increases the burning velocity. Likewise, 18 % of the N_2O is consumed through the related reactions of Fe or FeO with N_2O , reducing the N_2O consumption through both the direct reaction and reaction with O-atoms. While reaction of N_2O through the catalytic route with iron species or through the direct reaction with CO proceeds at roughly the same rate, reaction of N_2O with O-atoms is less exothermic than the direct reaction (because of the slow consumption of NO as shown in Figure 1), so reducing the importance of the O-

atom reactions with N_2O increases the burning velocity. Nonetheless, the effect of iron as a catalytic agent to reduce radical mole fractions is secondary in these flames.

As described in Ref. [25], $\text{Fe}(\text{CO})_5$ in moist $\text{CO-O}_2\text{-N}_2$ flames acts as a catalyst to recombine O atoms (as opposed to methane-air flames, where H-atom recombination appears to be the important inhibition reaction). These dry N_2O flames appear to be similar to the $\text{CO-H}_2\text{-O}_2\text{-N}_2$ flames in that iron species do serve to recombine O atoms. For example, with 213 ppm of $\text{Fe}(\text{CO})_5$, about 23% of the O-atom consumption occurs through reactions with iron intermediates. In this flame, however, a reduction in O-atom mole fraction leads to a slightly higher overall reaction rate. Very little of the CO consumption occurs via reaction with O atoms, but a reduced mole fraction of O reduces its reaction with N_2O . Nonetheless, the effect of O-atom recombination is minor, and the main influence of adding iron pentacarbonyl to the dry flames is to promote the N_2O reaction through the iron-catalyzed reaction sequence described above.

Moist Flames

The moist N_2O flames without $\text{Fe}(\text{CO})_5$ are described above and in Tables 4 and 5. Carbon monoxide is consumed by reaction with OH (60 %) and N_2O (38 %), and N_2O is consumed roughly equally by reaction with CO, H atom, O atom, and by thermal decomposition. With addition of iron species, the catalytic route described above again contributes to CO and N_2O consumption, but it is only about two-thirds as important as in the dry case (primarily because of the dominant role of the CO+OH and $\text{N}_2\text{O+H}$ reactions). The iron species do enter into catalytic recombination reactions for H and O atoms, but these cycles are not significant. For H and OH, less than 1 % of the flux of each involves iron-species reactions. For O atom, although iron-species reactions account for about 8 % of its consumption, the sensitivities (not shown in Table 5) indicate that consumption of O atoms by reaction with iron species increases the burning

velocity as described above. (For reference, Fe reactions in CO flames with 1 % hydrogen cause 30 % and 70 % of the H- and O-atom destruction at about 200 ppm of $\text{Fe}(\text{CO})_5$ [25], and about a 30 % reduction in the flame speed.)

In the present moist CO-N₂O flames, oxygen atom is not a significant species for CO consumption or in chain reactions. Hydrogen and hydroxyl radicals are important for consumption of N₂O and CO, but the system is straight-chain rather than chain-branching, and neither radical reaches very high concentrations (their estimated peak mole fractions in CH₄, O₂, and the present flames are listed in Table 1). The sensitivity of the burning velocity to the rate of the branching reaction O+H₂ is also low, ranking as the twelfth most sensitive reaction, as compared to methane-air or moist CO-air flames, where the burning velocity is very sensitive to the rate of the branching reaction H+O₂ (which is also not important in the present flames).

Hence, while there is some inhibition, the effect of the iron species is mostly to promote the overall reaction through the iron-catalyzed reactions of CO and N₂O described above. With H₂ addition the promotion is less pronounced, not because of significant hydrogen radical recombination by the iron species, but because the moist system is dominated by the fast OH+CO reaction, so the iron-catalyzed reactions account for less of the CO and N₂O consumption.

CONCLUSIONS

The first measurements of the burning velocity of CO-N₂O flames with low (13 ppm) levels of hydrogen-containing impurities have been obtained, for $0.6 \leq \phi \leq 3.0$ and with added nitrogen up to $X_{\text{N}_2} = 0.25$; data have also been collected for flames with added hydrogen up to $X_{\text{H}_2} = 0.005$. The measured burning velocity of pure stoichiometric flames is 23.1 cm/s +/- 0.6 cm/s, and the measurements with added hydrogen are in

good agreement with those of other researchers which were obtained at higher hydrogen mole fractions. The present data and those of earlier investigations were numerically modeled using a mechanism based on Allen et al. [1] with a CO+OH rate from Yu et al. [40], and the CO + N₂O direct reaction rate of Milks and Matula [6]. Modeling of the flames requires the use of the direct reaction, and the present results imply a rate of $10^{9.2} \text{ cm}^3 / \text{mol s}$ at 1800 K, which corresponds to a 10 % decrease in the pre-exponential factor of the Milks and Matula rate. Experiments with nitrogen dilution and over a range of ϕ suggest an activation energy near 71 kJ/mole. For dry flames with $0.6 \leq \phi \leq 3.0$, the mechanism overpredicts the burning velocity by about 18% for lean flames and underpredicts it by about 25% for rich flames. For the moist flames, the CO+OH rate also has a strong effect on the predicted burning velocity, and the rates of Yu et al. [40] or Wooldridge et al. [44] provide good agreement with our data.

Iron pentacarbonyl, which is the most effective flame inhibitor identified for hydrocarbon-air flames, is not effective in N₂O flames; in fact, 213 ppm of Fe(CO)₅ actually increases the burning velocity of the dry flames by about 25 %. The promotion is believed to be due to the iron-catalyzed gas-phase reaction of N₂O with CO, via $\text{N}_2\text{O} + \text{M} = \text{N}_2 + \text{MO}$ and $\text{CO} + \text{MO} = \text{CO}_2 + \text{M}$, where M is Fe, FeO, or FeOH. The rate expression of Plane and Rollason [50] for the former reaction with M=Fe, together with estimates of the rates of other reactions provide reasonable agreement with the present data. For moist CO – N₂O flames, the promotion provided by the iron pentacarbonyl is less pronounced, not because of radical recombination by the inhibitor, but because the iron-catalyzed reaction of CO and N₂O is of lesser importance relative to CO and N₂O reaction with OH and H, respectively.

The present results show that the extraordinary effectiveness of iron pentacarbonyl may be limited to systems in which the oxidizer is O₂. The findings

emphasize that unlike thermal diluents, the effect a chemical “inhibitor” will have on the overall reaction rate is highly dependent upon the chemical system involved. For example, for some propellant flames which release CO and N₂O in the gas phase, the most effective inhibitor found for hydrocarbon-air flames (Fe(CO)₅) would likely accelerate the burning, as may halogen-based inhibitors.

ACKNOWLEDGEMENTS

We are grateful to Dr. Richard Yetter for helpful discussions of N₂O kinetics and for providing his N₂O mechanism, to Dr. Pamela Chu for the FTIR analysis of N₂O and CO, and to Ms. Nikki Privé for assistance with the data acquisition and uncertainty analysis programs. The helpful conversations and encouragement of Dr. Wing Tsang of NIST contributed much to this research.

REFERENCES

- [1] Allen, M.T., Yetter, R.A., and Dryer, F.L., *Combust. Flame* 109:449 (1997).
- [2] Cor, J.J. and Branch, M.C., *J. Propul. Power* 11:704 (1995).
- [3] Litzinger, T.A., Fetherolf, B.L., Lee, Y.J., and Tang, C.J., *J. Propul. Power* 11:698 (1995).
- [4] Yetter, R.A., Dryer, F.L., Allen, M.T., and Gatto, J.L., *J. Propul. Power* 11:683 (1995).
- [5] Zaslonko, I.S., Losev, A.S., Mozzhukhin, E.V., and Mukoseev, Yu.K., *Kinetics and Catalysis* 20:1144 (1979).
- [6] Milks, D. and Matula, R., *Fourteenth Symposium (International) on Combustion*, The Combustion Institute, Pittsburgh, 1973, pp. 84.
- [7] Fujii, N., Kakuda, T., Takeishi, N., and Miyama, H., *J. Phys. Chem.* 91:2144 (1987).
- [8] Loirat, H., Caralp, F., and Destriau, M., *J. Phys. Chem.* 87:2455 (1983).
- [9] Dindi, H., Tsai, H.M., and Branch, M.C., *Combust. Flame* 87:13 (1991).
- [10] Vandooren, J., Van Tiggelen, P.J., and Pauwels, J.F., *Combust. Flame* 109:647 (1997).
- [11] Cor, J.J. and Branch, M.C., *Combust. Sci. Technol.* 127:71 (1997).
- [12] Van Wonterghem, J. and Van Tiggelen, A., *Bull. Soc. Chim. Belg.* 64:780 (1955).
- [13] Kalff, P.J. and Alkemade, C.Th.J., *Combust. Flame* 19:257 (1972).
- [14] Simpson, C.J.S.M. and Linnett, J.W., *Sixth Symposium (International) on Combustion*, Reinhold, New York, 1957, pp. 257-265.
- [15] Linteris, G.T. and Williams, F.A., *Twenty-Fourth Symposium (International) on Combustion*, The Combustion Institute, Pittsburgh, 1992, pp. 803-811.
- [16] Andersen, S.O., *Fire Journal* 81:56 (1987).
- [17] Gann, R. G. Ed., *Fire Suppression System Performance of Alternative Agents in Aircraft Engines and Dry Bay Laboratory Simulations*, National Institute of Standards and Technology, NIST SP 890, 1995.
- [18] Lask, G. and Wagner, H.G., *Eighth Symposium (International) on Combustion*, Williams and Wilkins Co., Baltimore, 1962, pp. 432-438.
- [19] Vanpee, M. and Shirodkar, P., *Seventeenth Symposium (International) on Combustion*, The Combustion Institute, Pittsburgh, 1979, pp. 787-795.
- [20] Miller, D.R., Evers, R.L., and Skinner, G.B., *Combust. Flame* 7:137 (1963).
- [21] Reinelt, D. and Linteris, G.T., *Twenty-Sixth Symposium (International) on Combustion*, The Combustion Institute, Pittsburgh, PA, 1996, pp. 1421-1428.
- [22] Linteris, G.T., Rumminger, M.D., Babushok, V.I., and Tsang, W., *Twenty-Eighth Symposium (International) on Combustion*, The Combustion Institute, Pittsburgh, PA, 1999, (submitted).
- [23] Rumminger, M.D., Reinelt, D., Babushok, V., and Linteris, G.T., *Combust. Flame* 116:207 (1999).
- [24] Rosser, W. A, Inami, S. H., and Wise, H., *Study of the Mechanisms of Fire*

- Extinguishment of Liquid Rocket Propellants*, WADC Technical Report 59-206, 1959.
- [25] Rumminger, M.D. and Linteris, G.T., *Combust. Flame* 120:451 (2000).
 - [26] Kaufman, F., *Proc. R. Soc. London, A* A247:123 (1958).
 - [27] Mache, H. and Hebra, A., *Sitzungsber. Österreich. Akad. Wiss. IIa*, 150:157 (1941).
 - [28] Van Wonterghem, J. and Van Tiggelen, A., *Bull. Soc. Chim. Belg.* 63:235 (1954).
 - [29] Andrews, G.E. and Bradley, D., *Combust. Flame* 18:133 (1972).
 - [30] Linteris, G.T. and Truett, L., *Combust. Flame* 105:15 (1996).
 - [31] Taylor, B. N. and Kuyatt, C. E., *Guidelines for Evaluating and Expressing the Uncertainty of NIST Measurement Results*, National Institute of Standards and Technology, NIST Technical Note 1297, 1994.
 - [32] Rumminger, M. D. and Linteris, G. T., *Inhibition of Premixed Carbon Monoxide-Hydrogen-Oxygen-Nitrogen Flames by Iron Pentacarbonyl*, National Institute of Standards and Technology, NIST IR 6360, 1999.
 - [33] Weinberg, F. J., *Optics of Flames*, Butterworth, London, 1963.
 - [34] Dunn-Rankin, D. and Weinberg, F., *Combust. Flame* 113:303 (1998).
 - [35] Fristrom, R.M., *Physics of Fluids* 8:273 (1965).
 - [36] Gilbert, A.G. and Sulzmann, K.G.P., *J. Electrochem. Soc.* 121:832 (1974).
 - [37] Kee, R. J., Grcar, J. F., Smooke, M. D., and Miller, J. A., *A Fortran Computer Program for Modeling Steady Laminar One-dimensional Premixed Flames*, Sandia National Laboratories Report, SAND85-8240, 1991.
 - [38] Kee, R. J., Rupley, F. M., and Miller, J. A., *CHEMKIN-II: A Fortran Chemical Kinetics Package for the Analysis of Gas Phase Chemical Kinetics*, Sandia National Laboratory, SAND89-8009B, 1989.
 - [39] Kee, R. J., Dixon-Lewis, G., Warnatz, J., Coltrin, R. E., and Miller, J. A., *A Fortran Computer Package for the Evaluation of Gas-Phase, Multicomponent Transport Properties*, Sandia National Laboratory, SAND86-8246, 1986.
 - [40] Yu, C.-L., Wang, C., and Frenklach, M., *Eastern States Section of the Combustion Institute*, The Combustion Institute, 1990, pp. 20-1 to 20-4.
 - [41] Loirat, H., Caralp, F., Destriau, M., and Lesclaux, R., *J. Phys. Chem.* 91:6538 (1987).
 - [42] Baulch, D. L., Drysdale, D. D., Horne, D. G., and Lloyd, A. C., *Evaluated Kinetic Data for High Temperature Reactions, vol. 1 and 2*, Butterworths, London, 1973.
 - [43] Baulch, D.L., Cobos, C.J., Cox, R.A., Esser, C., Frank, P., Just, T., Kerr, J.A., Pilling, M.J., Troe, J., Walker, R.W., and Warnatz, J., *J. Phys. Chem. Ref. Data* 21:411 (1992).
 - [44] Wooldridge, M.S., Hanson, R.K., and Bowman, C.T., *Twenty-Fifth Symposium (International) on Combustion*, The Combustion Institute, Pittsburgh, PA, 1994, pp. 741-748.
 - [45] Lin, M.C. and Bauer, S.H., *J. Phys. Chem.* 50:3377 (1969).
 - [46] Day, M.J., Stamp, D.V., Thompson, K., and Dixon-Lewis, G., *Thirteenth*

- Symposium (International) on Combustion*, The Combustion Institute, Pittsburgh, 1971, pp. 705-712.
- [47] Palmer, H.B. and Seery, D.J., *Combust. Flame* 4:213 (1960).
 - [48] West, J.B. and Broida, H.P., *J. Chem. Phys.* 62:2566 (1975).
 - [49] Campbell, M.L. and Metzger, J.R., *Chem. Phys. Lett.* 253:158 (1996).
 - [50] Plane, J.M.C. and Rollason, R.J., *J. Chem. Soc., Faraday Trans.* 92:4371 (1996).
 - [51] Kappes, M.M. and Staley, R.H., *Journal of the American Chemical Society* 103:1286 (1981).
 - [52] Matsuda, S., *J. Phys. Chem.* 57:807 (1972).
 - [53] Hayhurst, A.N. and Lawrence, A.D., *Combust. Flame* 110:351 (1997).
 - [54] Kellogg, C.B. and Irikura, K.K., *Journal of Physical Chemistry a* 103:1150 (1999).
 - [55] Rumminger, M.D. and Linteris, G.T., *Halon Options Technical Working Conference*, Albuquerque, NM, 1999, pp. 511-521.
 - [56] Rumminger, M.D. and Linteris, G.T., "An Experimental Study Of The Role Of Particles In Flame Inhibition By Iron Pentacarbonyl", submitted to *Combustion and Flame*, 1999.

TABLE CAPTIONS

- Table 1 - Calculated CO-N₂O flame properties for various reactant streams. Values for stoichiometric CH₄ – air and CO-air-H₂ flames are provided for comparison.
- Table 2 - Measured burning velocity of CO-N₂O flames. Data are presented for dry flames at varying equivalence ratio ϕ and for stoichiometric flames with varying % H₂ and % N₂.
- Table 3 - Reactions in the iron catalytic cycle for the CO-N₂O system, and their estimated reaction rates ($k_f = A T^b \exp(-E_a/RT)$), and units are cm, K, mole, s).
- Table 4 - Calculated fractional flux of the total reaction of each species proceeding through the indicated reaction for stoichiometric CO-N₂O flames. Results are given for $X_{H_2} = 0.0$ and 0.002, and for $X_{Fe(CO)_5} = 0$ and 213 ppm.
- Table 5 - Sensitivity of burning velocity to the specific reaction rate constant for stoichiometric CO-N₂O flames with $X_{H_2} = 0$ and 0.002, and for $X_{Fe(CO)_5} = 0$ ppm and 213 ppm. Sensitivities are normalized by the value for the maximum sensitivity, which is the direct CO+N₂O reaction.

FIGURE CAPTIONS

Figure 1 - Calculated major species mole fraction and temperature profiles in a stoichiometric premixed dry CO-N₂O flame (note log distance scale).

Figure 2 - Burning velocity of stoichiometric CO-N₂O flames as a function of hydrogen mole percent. Points (squares) are experimental data, and the solid lines are the modeling results using the rate of the CO+N₂O from the reference indicated in the figure. The data of Kalff and Alkemade [13] with H₂O (not H₂) are indicated by 'K(H₂O)' and diamonds, and the datum of Van Wonerghem and Van Tiggelen [12] by 'V' and a triangle.

Figure 3 - Calculated burning velocity (lines) of CO-N₂O flames with values of the CO+OH→CO₂+H rate from Baulch et al. [42], Yu et al. [40], Wooldridge et al. [44], and Baulch et al. [43], together with data from the present study (symbols).

Figure 4 - Arrhenius plots of the rate of the direct exchange reaction CO+N₂O → CO₂+N₂ from various investigators (k in cm, K, mole, s).

Figure 5 - Measured burning velocity (squares) and calculated results (lines) of CO-N₂O flames with added N₂. The solid lines correspond to the as given CO+N₂O rate of Milks and Matula [6] or Loirat et al., 1987 [41]; the dotted lines have the pre-exponential adjusted for agreement at X_{N₂}=0. Triangles are data from ref. [12], and dashed line has 1560 ppm H₂ and adjusted pre-exponential factor.

Figure 6 - Measured burning velocity (squares) and calculated results (lines) of CO-N₂O flames as a function of fuel-oxidizer equivalence ratio ϕ . The solid lines correspond to the CO+N₂O rate of Milks and Matula [6] or Loirat et al. [41] as given; the dotted lines have the pre-exponential adjusted for agreement at ϕ =1.0. Triangles are data from ref. [12], and dashed line has 1560 ppm H₂ and adjusted pre-exponential factor.

Figure 7 - Experimental burning velocity of CO-N₂O flames as a function of the mole percent H₂O in the reactants, from [14] for ϕ =2.0 and X_{N₂} = 0.25, together with numerically calculated prediction.

Figure 8 - Calculated flux of important CO (dotted lines) and N₂O reactions (solid lines) in a stoichiometric CO-N₂O flame as a function of mole percent of hydrogen.

Figure 9 - Calculated flux of important CO reactions (dotted lines) and N₂O reactions (solid lines) in a dry, stoichiometric CO-N₂O flame as a function of ϕ .

Figure 10 - Normalized burning velocity of stoichiometric CO-N₂O flames with X_{H₂} = 0.0, 0.001, and 0.002 for increasing quantities of Fe(CO)₅. The symbols are the experimental data; the lines are the calculated results.

TABLES

Table 1 - Calculated CO-N₂O flame properties for various reactant streams. Values for stoichiometric CH₄ – air and CO-air-H₂ flames are provided for comparison.

Reactant Conditions			Temperature (K)				Peak Radical Mole Fraction within Flame (ppm)		
ϕ	Mole % H ₂	Mole % N ₂	$v_{o, num}$ (cm/s)	A.F.T.	At Point of 99.5 % N ₂ O Consumption	At peak of CO+N ₂ O Reaction	O	OH (ppm)	H
CO – N ₂ O Flame									
1	0	0	24.5	2870	2323	1770	2833	0	0
1	0.012	0	25.9	2872	2377	1773	3524	79	2
1	0.68	0	45.0	2866	2589	1896	4524	1811	38
0.6	0	0	20.1	2789	2303	1693	2690	0	0
1	0	0	24.5	2860	2324	1770	2833	0	0
1.3	0	0	25.7	2867	2319	1789	2710	0	0
3.2	0	0	22.1	2378	2139	1658	1109	0	0
1	0	0	24.5	2860	2323	1770	2833	0	0
1	0	25	16.6	2559	2155	1737	1590	0	0
CH ₄ - air Flame									
1	-	-	40.0	2230	-	-	3150	7660	6740
CO–air-H ₂ Flame									
1	1.0	-	35.8	2376	-	-	14000	5200	2900

Table 2 - Measured burning velocity of CO-N₂O flames. Data are presented for dry flames at varying equivalence ratio ϕ and for stoichiometric flames with varying % H₂ and % N₂.

ϕ	$v_{o,exp}$ (cm/s)	Mole % H ₂ ($\phi = 1.0$)	$v_{o,exp}$ (cm/s)	Mole % N ₂ ($\phi = 1.0$)	$v_{o,exp}$ (cm/s)
0.60	16.3 ± 0.4	0.00	23.4 ± 0.6	0.0	23.7 ± 0.6
0.75	19.9 ± 0.5	0.10	31.9 ± 0.8	2.5	22.2 ± 0.6
0.80	20.8 ± 0.5	0.15	35.9 ± 1.1	5.3	22.8 ± 0.6
0.85	21.6 ± 0.5	0.20	38.7 ± 1.2	8.1	22.2 ± 0.6
0.90	22.2 ± 0.5	0.25	41.8 ± 1.6	11.1	21.7 ± 0.6
0.95	22.7 ± 0.6	0.30	44.8 ± 1.5	14.3	20.9 ± 0.6
1.0	23.4 ± 0.6	0.32	44.6 ± 1.7	17.7	20.2 ± 0.6
1.1	24.4 ± 0.6	0.35	46.9 ± 2.0	21.3	19.3 ± 0.5
1.2	25.5 ± 0.6	0.40	48.2 ± 2.5	25.1	17.9 ± 0.6
1.3	26.3 ± 0.7	0.45	49.3 ± 2.3		
1.5	27.6 ± 0.7	0.50	51.8 ± 3.4		
1.8	28.4 ± 0.7				
2.1	28.8 ± 0.7				
2.5	28.4 ± 0.7				
3.0	27.3 ± 0.7				

Table 3 - Reactions in the iron catalytic cycle for the CO-N₂O system, and their estimated reaction rates ($k_f = A T^b \exp(-E_a/RT)$, and units are cm, K, mole, s).

<i>Reaction</i>	<i>A</i>	<i>b</i>	<i>E_a/R</i>
Fe + N ₂ O = FeO + N ₂	1.40 E+14	0	5940
FeO + N ₂ O = FeO ₂ + N ₂	3.00 E+13	0	5033
FeOH + N ₂ O = FeOOH + N ₂	1.30 E+14	0	4530
FeO + CO = Fe + CO ₂	1.80 E+12	0	3522
FeO ₂ + CO = FeO + CO ₂	1.18 E+13	0	4530
FeOOH + CO = FeOH + CO ₂	6.00 E+13	0	4026

Table 4 - Calculated fractional flux of the total reaction of each species proceeding through the indicated reaction for stoichiometric CO-N₂O flames. Results are given for X_{H₂} = 0.0 and 0.002, and for X_{Fe(CO)₅} = 0 and 213 ppm.

		Fractional Flux (%)			
		X _{H₂} :			
		0.000		0.002	
		X _{Fe(CO)₅} (ppm):			
		0	213	0	213
Species	Reaction				
CO	Destruction				
	CO + OH <=> CO ₂ + H	-	-	60	48
	CO + N2O <=> CO ₂ + N ₂	94	68	38	30
	CO + O(+M) <=> CO ₂ (+M)	3	0	1	0
	CO + NO ₂ <=> CO ₂ + NO	2	-	-	-
	FeO + CO <=> Fe + CO ₂	-	9	-	3
	FeO ₂ + CO <=> FeO + CO ₂	-	23	-	6
	FeOOH + CO <=> FeOH + CO ₂	-	-	-	12
N ₂ O	Destruction				
	CO + N ₂ O <=> CO ₂ + N ₂	40	30	19	16
	N ₂ O (+M) <=> N ₂ + O(+M)	31	30	26	26
	N ₂ O + H <=> N ₂ + OH	-	-	28	20
	N ₂ O + O <=> O ₂ + N ₂	13	10	11	10
	N ₂ O + O <=> 2NO	13	10	11	10
	NH + NO <=> N ₂ O + H	0	0	3	3
	NO + N ₂ O <=> NO ₂ + N ₂	2	1	1	1
	FeO + N ₂ O <=> FeO ₂ + N ₂	-	12	-	5
	Fe + N ₂ O <=> FeO + N ₂	-	6	-	4
	FeOH + N ₂ O <=> FeOOH + N ₂	-	-	-	6
O	Creation				
	N ₂ O(+M) <=> N ₂ + O(+M)	99	99	95	88
	H + O ₂ <=> O + OH	-	-	4	11
	Destruction				
	N ₂ O + O <=> O ₂ + N ₂	44	36	42	36
	N ₂ O + O <=> 2NO	44	36	42	36
	H + O ₂ <=> O + OH	-	-	6	2
	NH + O <=> NO + H	-	-	4	4
	CO + O(+M) <=> CO ₂ (+M)	4	2	2	2
	NO2 + O <=> O ₂ + NO	5	3	1	1
	NO + O (+M) <=> NO ₂ (+M)	2	-	-	-
	O + H ₂ <=> H + OH	-	-	1	1

	$\text{Fe} + \text{O}_2 \rightleftharpoons \text{FeO} + \text{O}$	-	12	-	9
	$\text{FeO}_2 + \text{O} \rightleftharpoons \text{FeO} + \text{O}_2$	-	11	-	7
H	Creation				
	$\text{CO} + \text{OH} \rightleftharpoons \text{CO}_2 + \text{H}$	-	-	87	89
	$\text{H} + \text{O}_2 \rightleftharpoons \text{O} + \text{OH}$	-	-	4	2
	$\text{NH} + \text{O} \rightleftharpoons \text{NO} + \text{H}$	-	-	3	3
	$\text{NH} + \text{NO} \rightleftharpoons \text{N}_2\text{O} + \text{H}$	-	-	3	3
	$\text{O} + \text{H}_2 \rightleftharpoons \text{H} + \text{OH}$	-	-	1	1
	Destruction				
	$\text{N}_2\text{O} + \text{H} \rightleftharpoons \text{N}_2 + \text{OH}$	-	-	83	73
	$\text{NH} + \text{NO} \rightleftharpoons \text{N}_2\text{O} + \text{H}$	-	-	10	10
	$\text{H} + \text{O}_2 \rightleftharpoons \text{O} + \text{OH}$	-	-	3	12
	$\text{NO}_2 + \text{H} \rightleftharpoons \text{NO} + \text{OH}$	-	-	3	3
OH	Creation				
	$\text{N}_2\text{O} + \text{H} \rightleftharpoons \text{N}_2 + \text{OH}$	-	-	87	77
	$\text{H} + \text{O}_2 \rightleftharpoons \text{O} + \text{OH}$	-	-	3	13
	$\text{NH} + \text{NO} \rightleftharpoons \text{N}_2 + \text{OH}$	-	-	3	3
	$\text{NO}_2 + \text{H} \rightleftharpoons \text{NO} + \text{OH}$	-	-	3	3
	$\text{H}_2\text{O} + \text{O} \rightleftharpoons 2\text{OH}$	-	-	1	2
	$\text{O} + \text{H}_2 \rightleftharpoons \text{H} + \text{OH}$	-	-	1	1
	Destruction				
	$\text{CO} + \text{OH} \rightleftharpoons \text{CO}_2 + \text{H}$	-	-	93	95
	$\text{H} + \text{O}_2 \rightleftharpoons \text{O} + \text{OH}$	-	-	5	2
	$\text{H}_2\text{O} + \text{O} \rightleftharpoons 2\text{OH}$	-	-	1	-
Fe	Creation				
	$\text{FeO} + \text{CO} \rightleftharpoons \text{Fe} + \text{CO}_2$	-	53	-	35
	$\text{Fe} + \text{O}_2 \rightleftharpoons \text{FeO} + \text{O}$	-	45	-	54
	$\text{Fe} + \text{O}_2 (+\text{M}) \rightleftharpoons \text{FeO}_2 (+\text{M})$	-	-	-	6
	$\text{FeO} + \text{H} \rightleftharpoons \text{Fe} + \text{OH}$	-	-	-	3
	Destruction				
	$\text{Fe} + \text{N}_2\text{O} \rightleftharpoons \text{FeO} + \text{N}_2$	-	85	-	88
	$\text{Fe} + \text{O}_2 (+\text{M}) \rightleftharpoons \text{FeO}_2 (+\text{M})$	-	14	-	11
FeO	Creation				
	$\text{Fe} + \text{N}_2\text{O} \rightleftharpoons \text{FeO} + \text{N}_2$	-	33	-	42
	$\text{FeO}_2 + \text{O} \rightleftharpoons \text{FeO} + \text{O}_2$	-	16	-	20
	$\text{FeO}_2 + \text{CO} \rightleftharpoons \text{FeO} + \text{CO}_2$	-	51	-	35
	Destruction				
	$\text{FeO} + \text{CO} \rightleftharpoons \text{Fe} + \text{CO}_2$	-	21	-	17
	$\text{FeO} + \text{N}_2\text{O} \rightleftharpoons \text{FeO}_2 + \text{N}_2$	-	62	-	53
	$\text{Fe} + \text{O}_2 \rightleftharpoons \text{FeO} + \text{O}$	-	18	-	26
	$\text{FeO} + \text{H} \rightleftharpoons \text{Fe} + \text{OH}$	-	-	-	2
	$\text{FeO} + \text{H}_2\text{O} \rightleftharpoons \text{Fe}(\text{OH})_2$	-	-	-	1

Table 5 - Sensitivity of burning velocity to the specific reaction rate constant for stoichiometric CO-N₂O flames with X_{H₂} = 0 and 0.002, and for X_{Fe(CO)₅} = 0 ppm and 213 ppm. Sensitivities are normalized by the value for the maximum sensitivity, which is the direct CO+N₂O reaction.

		$\frac{d(\ln v)/d(\ln k)}{d(\ln v)/d(\ln k) _{\max}}$			
		$X_{H_2} :$			
		<u>0</u>		<u>0.002</u>	
$X_{Fe(CO)_5}$ (ppm):		<u>0</u>	<u>213</u>	<u>0</u>	<u>213</u>
Reaction					
Dry Reactions					
CO + N ₂ O \rightleftharpoons CO ₂ + N ₂		1.00	1.00	1.00	1.00
N ₂ O (+M) \rightleftharpoons N ₂ + O (+M)		-0.13	-0.13	0.19	-0.10
N ₂ O + O \rightleftharpoons 2NO		-0.07	-0.07	-0.34	-0.23
N ₂ O + O \rightleftharpoons O ₂ + N ₂		0.00	0.04	0.04	0.06
Moist Reactions					
CO + OH \rightleftharpoons CO ₂ + H				0.83	0.63
N ₂ O + H \rightleftharpoons N ₂ + OH				0.32	0.31
H ₂ O + O \rightleftharpoons 2OH				-0.10	-0.06
O+ H ₂ \rightleftharpoons H + OH				0.09	0.09
Iron Reactions					
FeO ₂ + CO \rightleftharpoons FeO + CO ₂			0.30		0.28
FeO + CO \rightleftharpoons Fe+CO ₂			0.09		0.04
FeO + N ₂ O \rightleftharpoons FeO ₂ + N ₂			0.14		-0.05
Fe + N ₂ O \rightleftharpoons FeO+N ₂			0.02		0.04
FeOH + N ₂ O \rightleftharpoons FeOOH + N ₂					0.44
FeOOH + CO \rightleftharpoons FeOH + CO ₂					0.25
FeO + H ₂ O \rightleftharpoons Fe(OH) ₂					0.21
FeOH + H \rightleftharpoons FeO + H ₂					0.20
Fe(OH) ₂ + H \rightleftharpoons FeOH + H ₂ O					0.13
FeOH + O \rightleftharpoons FeO + OH					-0.08
FeOOH + OH \rightleftharpoons FeO ₂ + H ₂ O					-0.04

FIGURES

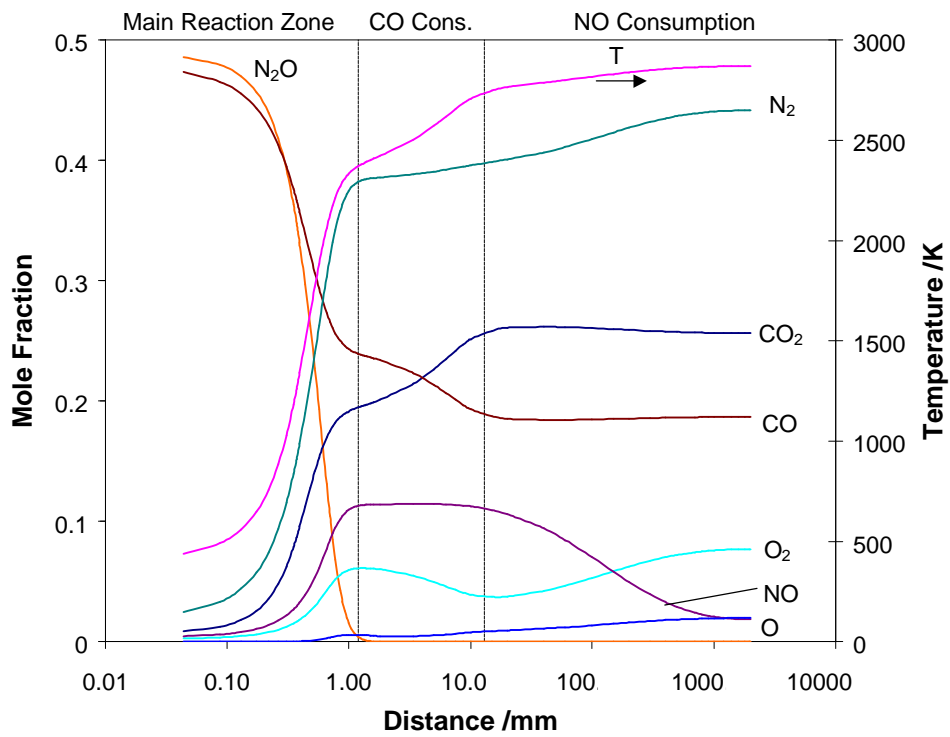


Figure 1 - Calculated major species mole fraction and temperature profiles in a stoichiometric premixed dry CO-N₂O flame (note log distance scale).

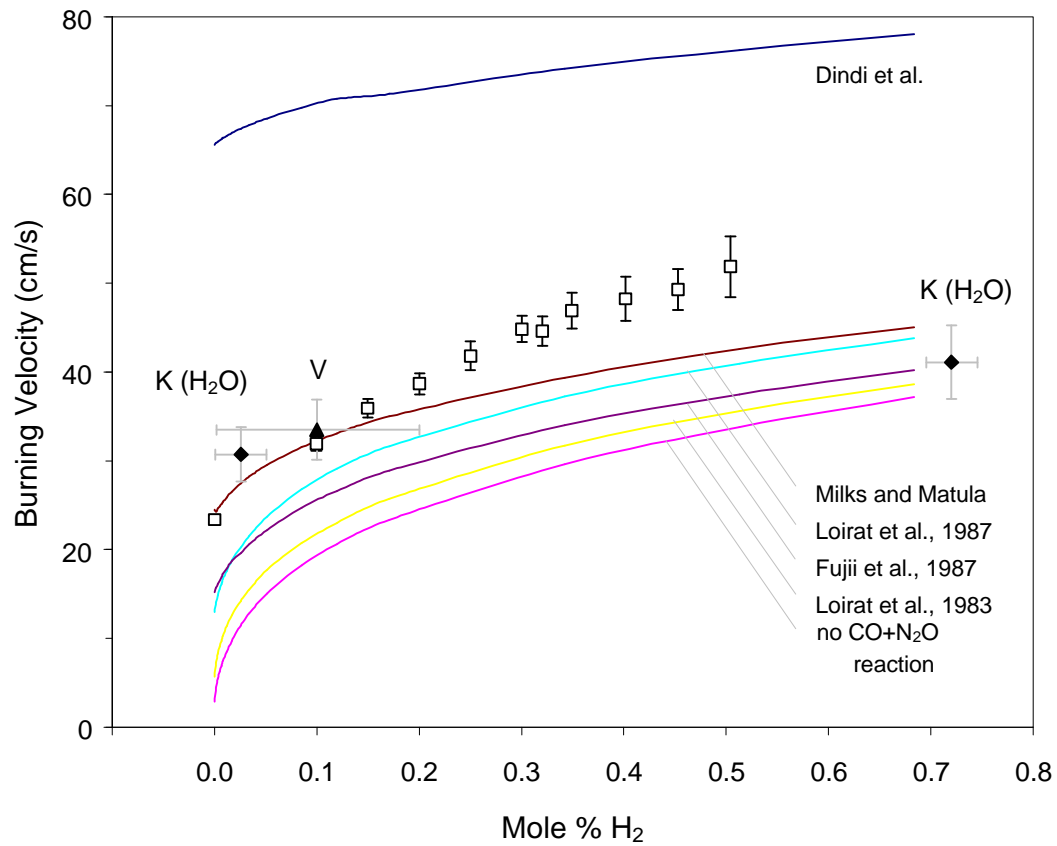


Figure 2 - Burning velocity of stoichiometric CO-N₂O flames as a function of hydrogen mole percent. Points (squares) are experimental data, and the solid lines are the modeling results using the rate of the CO+N₂O from the reference indicated in the figure. The data of Kalff and Alkemade [13] with H₂O (not H₂) are indicated by 'K(H₂O)' and diamonds, and the datum of Van Wonerghem and Van Tiggelen [12] by 'V' and a triangle.

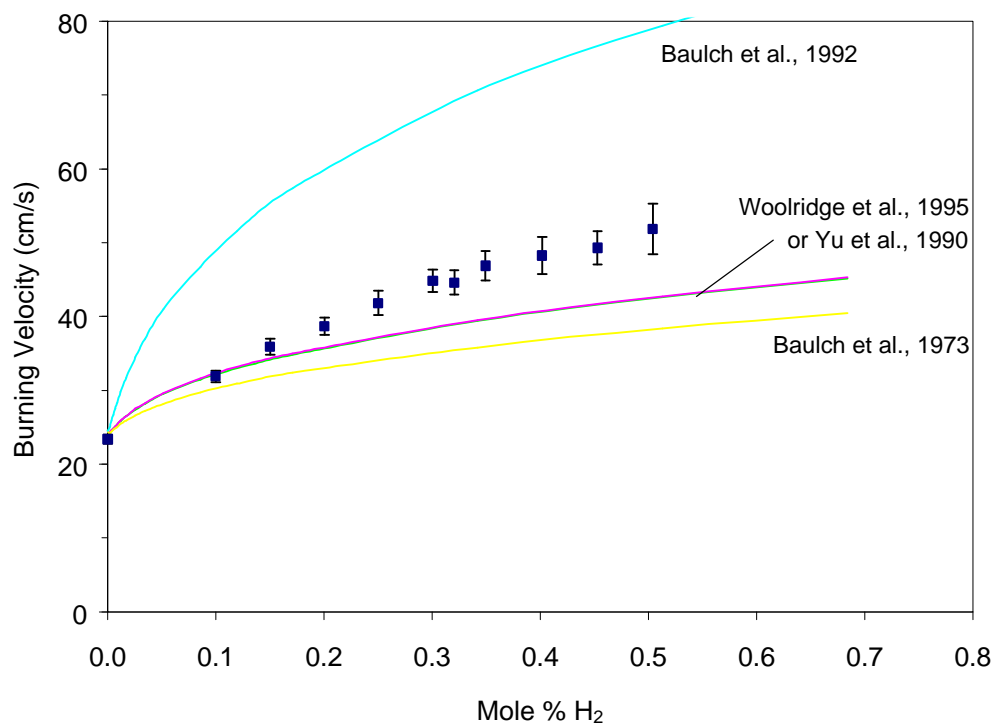


Figure 3 - Calculated burning velocity (lines) of CO-N₂O flames with values of the CO+OH→CO₂+H rate from Baulch et al. [42], Yu et al. [40], Wooldridge et al. [44], and Baulch et al. [43], together with data from the present study (symbols).

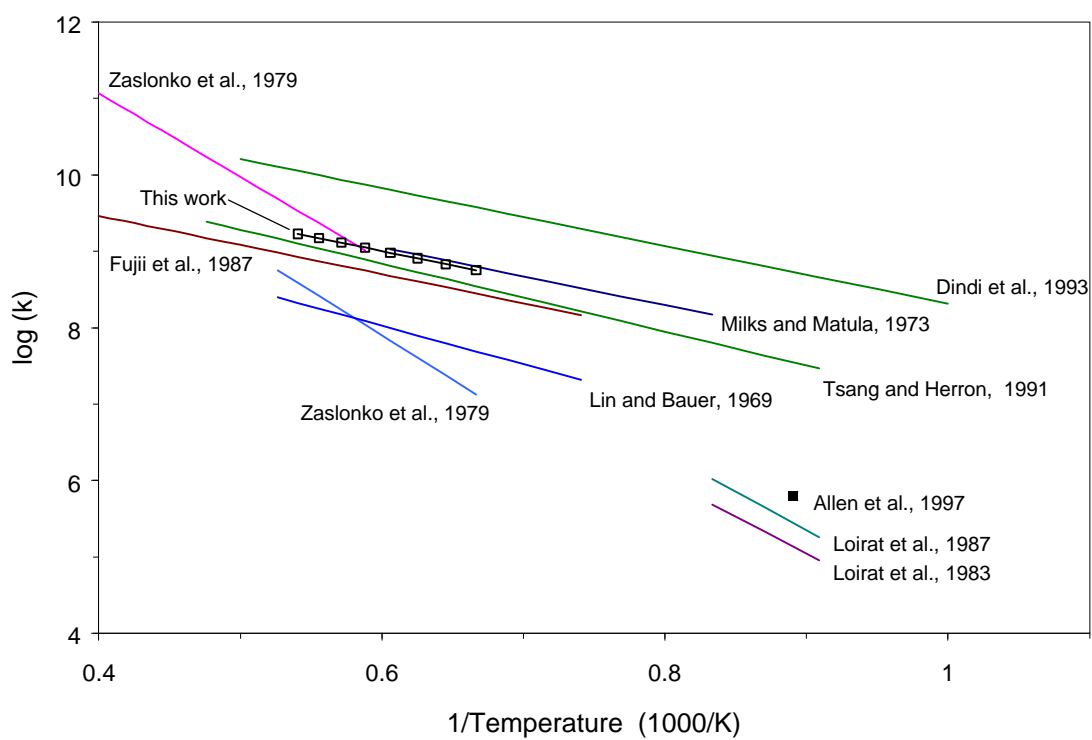


Figure 4 - Arrhenius plots of the rate of the direct exchange reaction $\text{CO} + \text{N}_2\text{O} \rightarrow \text{CO}_2 + \text{N}_2$ from various investigators (k in cm³ K mole⁻¹ s⁻¹).

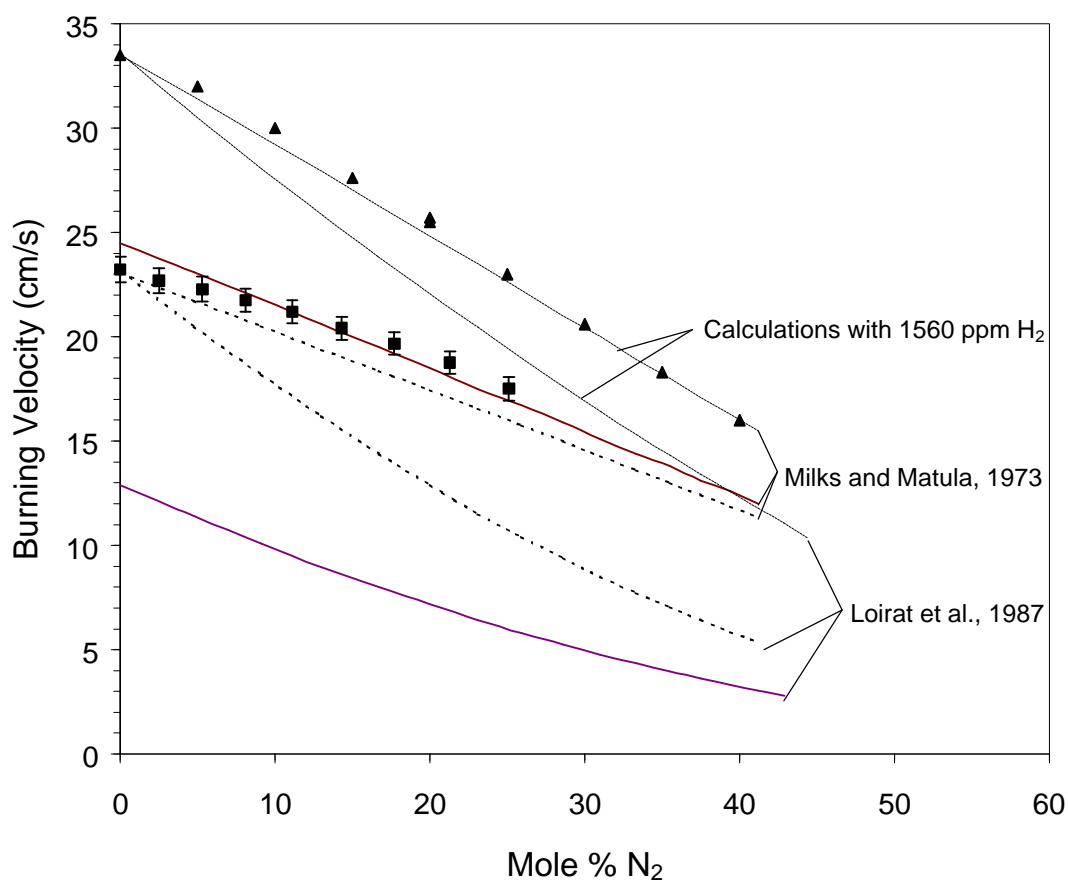


Figure 5 - Measured burning velocity (squares) and calculated results (lines) of CO-N₂O flames with added N₂. The solid lines correspond to the as given CO+N₂O rate of Milks and Matula [6] or Loirat et al., 1987 [41]; the dotted lines have the pre-exponential adjusted for agreement at $X_{N_2}=0$. Triangles are data from ref. [12], and dashed line has 1560 ppm H₂ and adjusted pre-exponential factor.

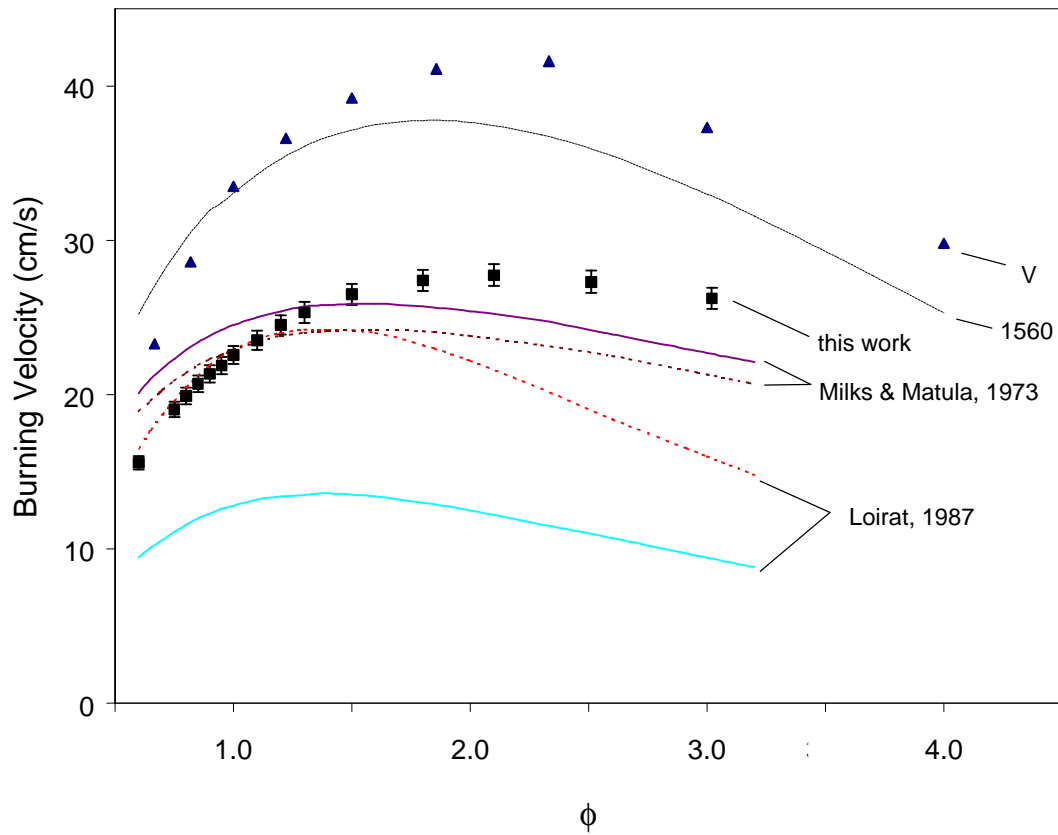


Figure 6 - Measured burning velocity (squares) and calculated results (lines) of CO-N₂O flames as a function of fuel-oxidizer equivalence ratio ϕ . The solid lines correspond to the CO+N₂O rate of Milks and Matula [6] or Loirat et al. [41] as given; the dotted lines have the pre-exponential adjusted for agreement at $\phi=1.0$. Triangles are data from ref. [12], and dashed line has 1560 ppm H₂ and adjusted pre-exponential factor.

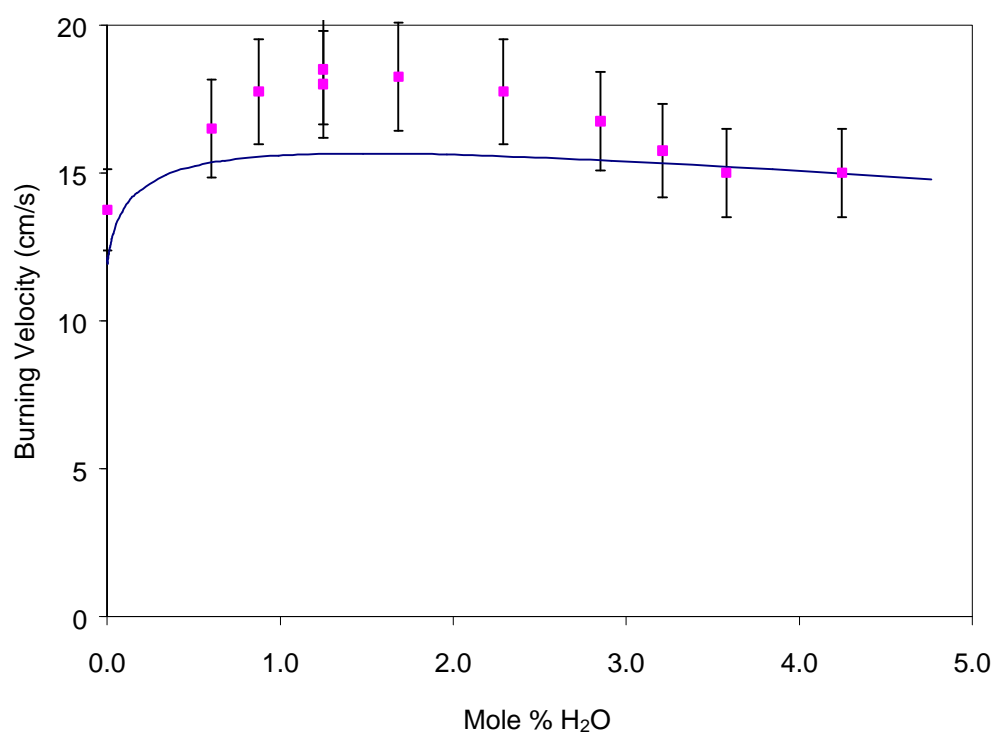


Figure 7 - Experimental burning velocity of CO-N₂O flames as a function of the mole percent H₂O in the reactants, from [14] for $\phi = 2.0$ and $X_{N_2} = 0.25$, together with numerically calculated prediction.

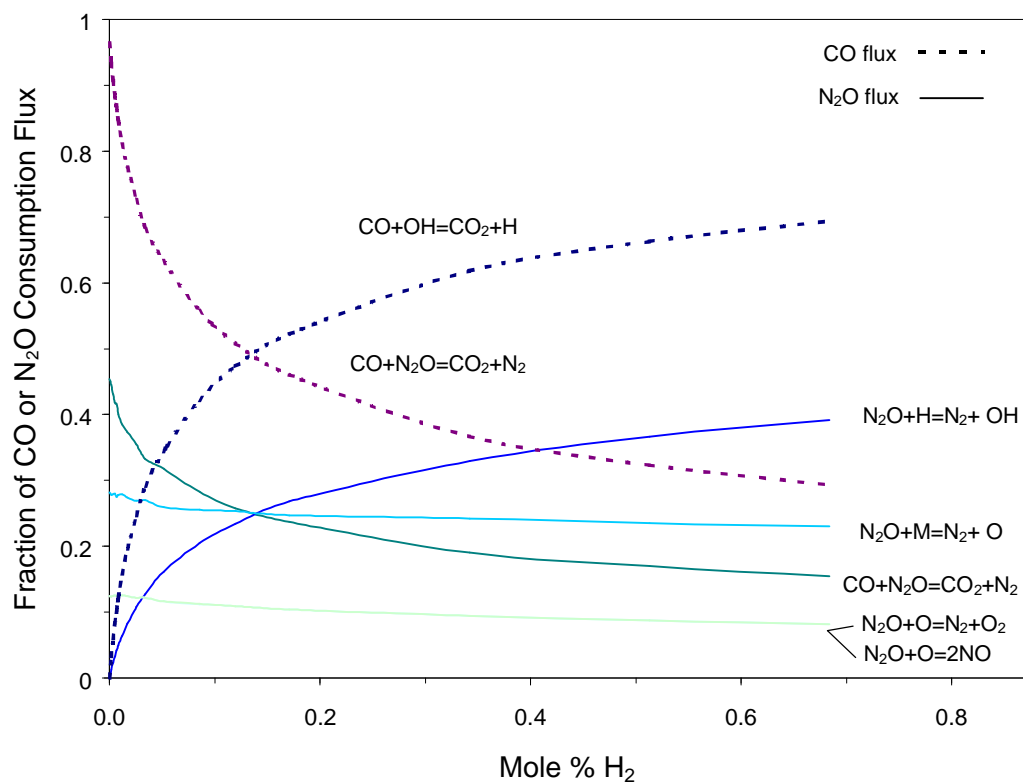


Figure 8 - Calculated flux of important CO (dotted lines) and N₂O reactions (solid lines) in a stoichiometric CO-N₂O flame as a function of mole percent of hydrogen.

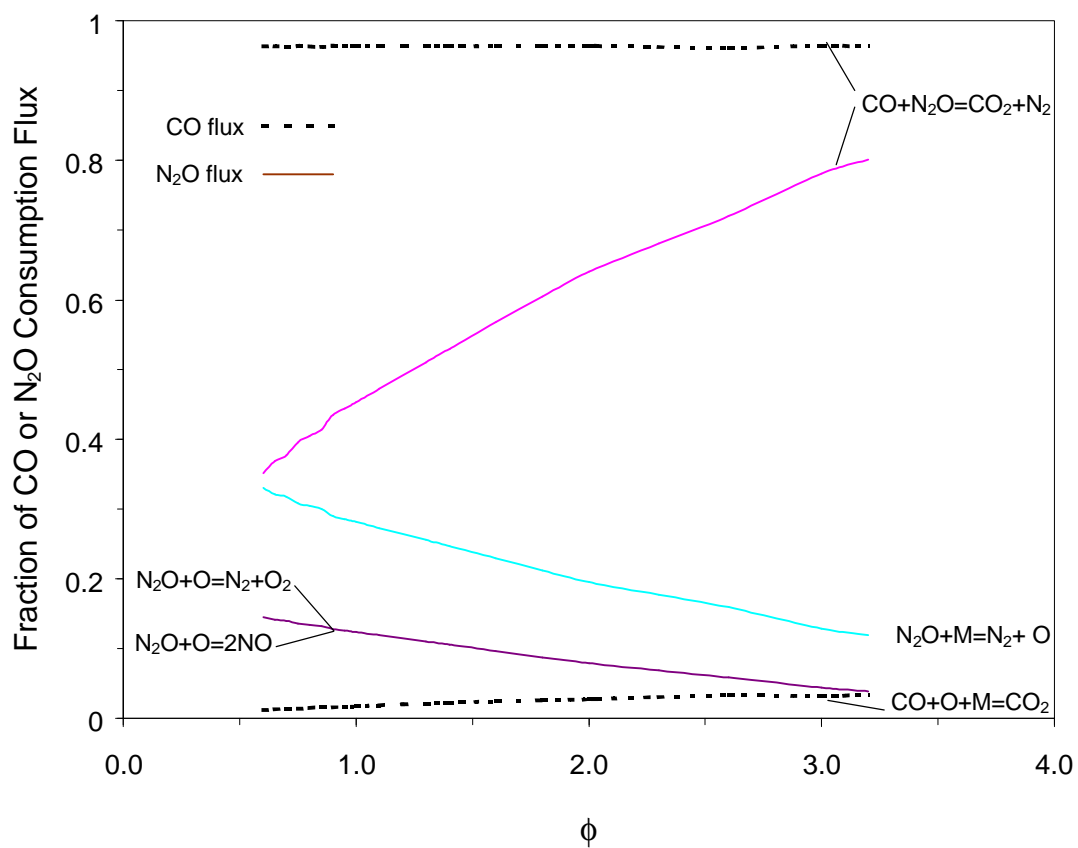


Figure 9 - Calculated flux of important CO reactions (dotted lines) and N₂O reactions (solid lines) in a dry, stoichiometric CO-N₂O flame as a function of ϕ .

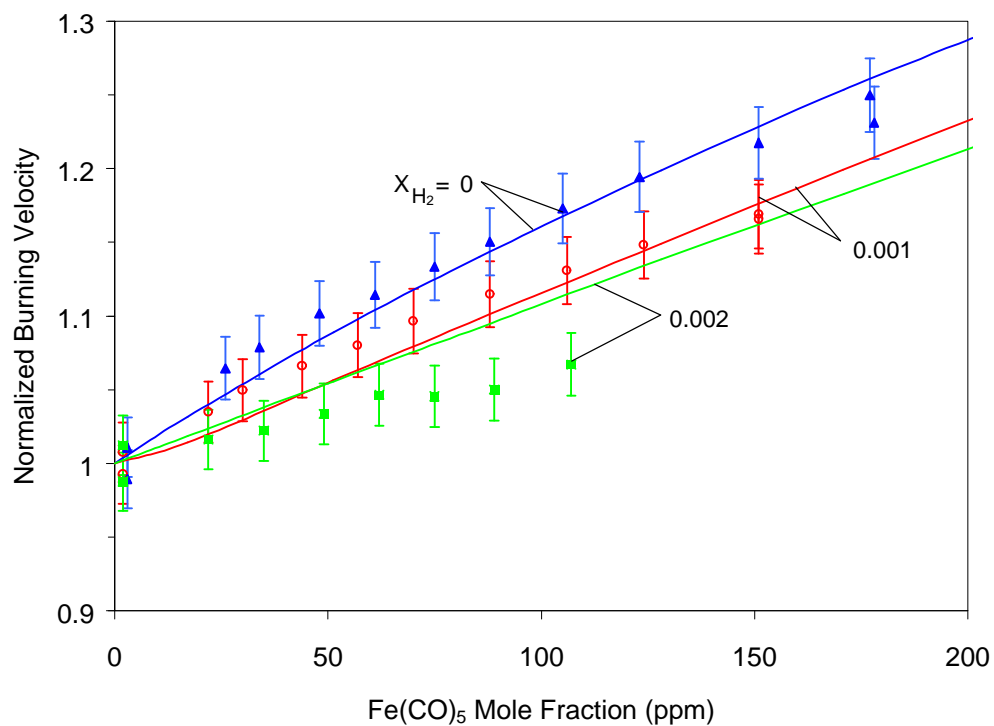


Figure 10 - Normalized burning velocity of stoichiometric CO-N₂O flames with $X_{H_2} = 0.0$, 0.001, and 0.002 for increasing quantities of Fe(CO)₅. The symbols are the experimental data, the lines are the calculated results.